Spatio-temporal image registration for respiratory motion correction in PET

Wenjia Bai and Sir Michael Brady*

Wolfson Medical Vision Laboratory, Department Of Engineering, University Of Oxford

Abstract. Positron emission tomography (PET) is a molecular imaging technique which is now widely established as a powerful tool for diagnosing a variety of cancers. However, PET images are substantially degraded by respiratory motion, to the extent that this may adversely impact upon subsequent diagnosis and patient management. A spatio-temporal image registration algorithm is proposed to align the moving images and correct for motion. Compared to conventional spatial registration, the proposed algorithm could yield better motion estimates. Experimental results show that motion correction using the spatio-temporal registration algorithm significantly improves PET image quality.

1 INTRODUCTION

Positron emission tomography (PET) is a molecular imaging technique which provides important functional information about the human body, especially about the metabolism of radioligands, and it is now widely established as a powerful tool for diagnosing a variety of cancers [1]. Combined with the anatomical information provided by CT, PET/CT has been shown to significantly increase diagnostic accuracy compared to using CT alone [2, 3].

However, PET images are substantially degraded by respiratory motion to the extent that this may, particularly for thoracic imaging, adversely impact upon subsequent diagnosis and patient management. In terms of the magnitude of motion, the diaphragm typically moves about 15-20 mm due to respiration; since current PET scanners have a spatial resolution of approximately 3-5 mm full width half maximum (FWHM), respiration substantially reduces the effective spatial resolution. In addition, it reduces the utility and reliability of subsequent image analysis and diagnosis. Studies have shown that the motion of the lungs can introduce artefacts and lead to incorrect judgements about lesions [4].

Gated acquisition of PET data has been proposed to overcome respiratory motion effects. Typically, a respiratory cycle is divided into a number of gates, during each of which the imaged object is assumed to be static. PET data for each gate are then collected and reconstructed separately. In order to maintain the count of coincidence events, all of the reconstructed gated images need to be aligned to the same position and then summed.

Several different approaches have been proposed to register the PET images. Lamare et al. proposed a B-spline deformable algorithm for image registration [5]. Dawood et al. compared a range of different optic flow algorithms for motion estimation [6]. However, these studies only utilise the spatial information in PET images for registration. The PET image for each gate is handled separately. As the respiratory motion is a continuous process, the PET images, considered across all the gates, also form a continuous change over time. Based on this assumption, we incorporate the temporal information into B-spline deformable registration in order to improve the registration accuracy. The work presented here extends the method developed in [7] for 2-D ultrasound image registration to a new application, namely 3-D PET image registration.

To validate our spatio-temporal B-spline registration algorithm, we used highly realistic, though simulated PET data (produced by PET-SORTEO), for which ground truth is available. Experimental results show that spatio-temporal registration could yield better motion estimates than spatial registration alone. In addition, motion correction using our registration algorithm significantly improves the resulting image quality. In this way, the PET images generated by our method can provide improved information for clinicians in cancer diagnosis and patient management.

2 METHODS

2.1 PET gating and motion correction scheme

Figure 1 illustrates the PET gating and motion correction scheme. The PET data is reconstructed for each gate. One of the reconstructed gated images is chosen to be the "reference" image, the other images being regarded as "test"

*Email: wenjia, jmb@robots.ox.ac.uk

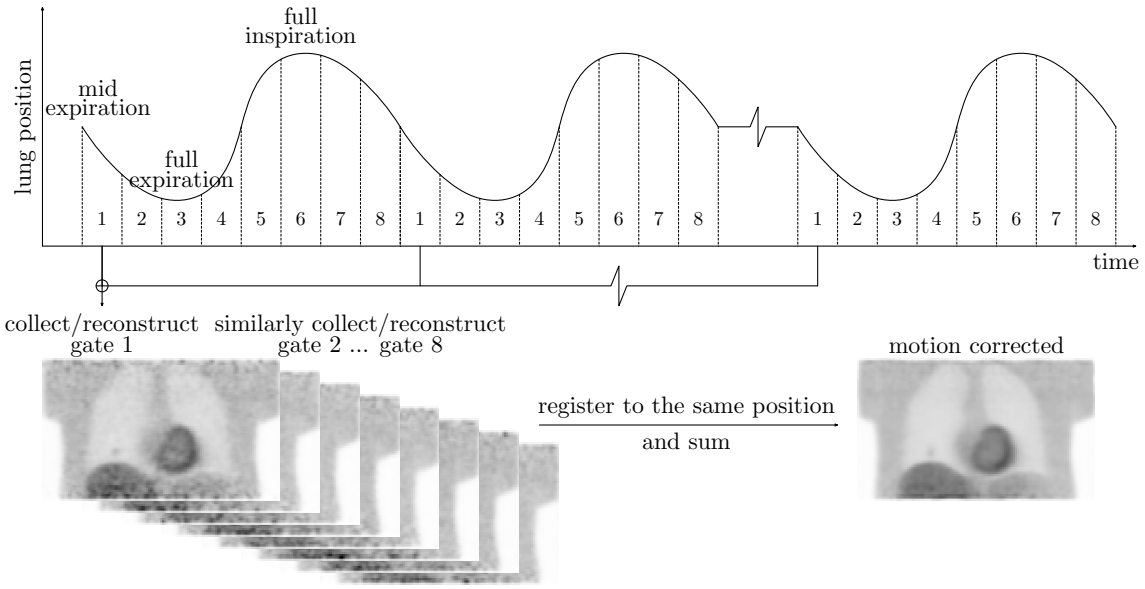

Figure 1. PET gating and motion correction scheme. A respiratory cycle is equally divided into 8 gates, in which the first gate corresponds to mid-expiration, the third and sixth gates correspond to full expiration and full inspiration respectively. The reconstructed images for each gate are registered to the same position and summed for motion correction.

images. We select the first gate f_1 to be the reference image, since it is in the middle of expiration and the average motion between the first gate and all the other gates is minimal. The other gates f_i $(2 \leq i \leq N)$ are regarded as test images.

Our algorithm registers each of the test images to the reference image so that the motion between different gates is estimated. In order to correct for the motion, we sum the registered images. In the following sections, we first introduce B-spline deformable registration using spatial information only [8], which separately registers each test image to the reference image. Then, we describe our spatio-temporal B-spline registration, which simultaneously registers all the test images to the reference image.

2.2 Spatial registration

The goal of registration is to find a transformation $g : x \rightarrow g(x|\mu)$ which maps the reference image $f_1(x)$ to a test image $f_i(x)$ so that $f_1(x)$ corresponds to $f_i(g(x|\mu))$ at each location, where $x \in \Omega$ denotes a pixel in a 3-D PET image, and μ denotes a 3-D vector-valued grid. Registration is formulated as an optimisation problem, where a cost function which measures the discrepancy between the reference image $f_1(x)$ and the transformed test image $f_i(g(x|\mu))$ is minimised with respect to μ, which has to be estimated.

Currently, we use the correlation coefficient (CC) as the cost function, since it has the merits of both mathematical simplicity and computational efficiency. The cost function of spatial registration is formulated as,

$$E_i(\mu) = \frac{n \sum f_1(x) f_i(g(x|\mu)) - \sum f_1(x) \sum f_i(g(x|\mu))}{\sqrt{n \sum f_1^2(x) - (\sum f_1(x))^2} \sqrt{n \sum f_i^2(g(x|\mu)) - (\sum f_i(g(x|\mu)))^2}} \tag{1}$$

where the summations are performed over all the pixels in the 3-D image, and n denotes the number of pixels. The local deformation $g(x|\mu)$ is determined by the weighted sum of the vectors on the grid μ,

$$g(x|\mu) = x + d(x|\mu) = x + \sum_{u \in S(x)} w(x,u)\mu(u) \tag{2}$$

where $d(x|\mu)$ denotes the displacement, $S(x)$ denotes the spatial support region of pixel x, $w(x,u)$ denotes the weight, and $\mu(u)$ denotes the vector at a control point u. By "support region", we mean the region within which the weight function is non-zero. The weight is defined as follows,

$$w(x,u) = \prod_{m=1}^{3} b^{(3)}(\frac{x_m}{h_{s,m}} - u_m) \tag{3}$$

where $b^{(3)}(\cdot)$ denotes the cubic B-spline function, h_s denotes the spacing of the 3-D grid μ, and m denotes the component of the 3-D coordinate. Since $g(x|\mu)$ does not necessarily coincide with a pixel lattice, image interpolation is required to evaluate the cost function. Image interpolation is also performed using cubic B-splines.

2.3 Spatio-temporal registration

Our algorithm for spatio-temporal B-spline registration takes account of the reference image $f_1(x)$ and all the test images $f_i(x)$ $(2 \leq i \leq N)$ in a single cost function,

$$E(\mu) = \frac{1}{N-1} \sum_{i=2}^{N} \frac{n \sum f_1(x) f_i(g(x|\mu)) - \sum f_1(x) \sum f_i(g(x|\mu))}{\sqrt{n \sum f_1^2(x) - (\sum f_1(x))^2} \sqrt{n \sum f_i^2(g(x|\mu)) - (\sum f_i(g(x|\mu)))^2}} \tag{4}$$

where $g(x, i|\mu)$ denotes the deformation vector at pixel x and gate i, and μ denotes the 4-D spatio-temporal vector-valued grid. The deformation $g(x, i|\mu)$ is determined by the weighted sum of the vectors on the grid μ,

$$g(x, i|\mu) = x + d(x, i|\mu) = x + \sum_{j \in T(i)} \sum_{u \in S(x)} w(i, j) w(x, u) \mu(u, j) \tag{5}$$

where $d(x, i|\mu)$ denotes the displacement, $T(i)$ denotes the temporal support region of i, $S(x)$ denotes the spatial support region of pixel x, $w(i, j)$ and $w(x, u)$ denote the corresponding weights, and $\mu(u, j)$ denotes the vector at a control point. The weights are also defined by cubic B-splines,

$$w(i, j) = b^{(3)}(\frac{i}{h_t} - j) \tag{6}$$

$$w(x, u) = \prod_{m=1}^{3} b^{(3)}(\frac{x_m}{h_{s,m}} - u_m) \tag{7}$$

where h_t and h_s denote the temporal and spatial spacing of the grid μ. Due to the periodicity of respiratory motion, the temporal weight function is also periodic,

$$w(i, j) = w(i, j + N) \tag{8}$$

In addition, since the first gate is regarded the reference gate, we have the constraint that the deformation vector $g(x, i|\mu)$ is zero for $i = 1$,

$$g(x, i|\mu) = 0, \text{if } i = 1 \tag{9}$$

2.4 Optimisation

Mathematically, image registration amounts to an optimisation problem. The cost function is minimised using gradient descent so that the deformation parameter μ is updated simultaneously at all the control points. The gradient is straightforward to derive from the cost function using the chain rule. The step size is estimated adaptively during each iteration [8]. The initial grid μ is set to a zero-valued array and the optimisation is terminated either after a minimal incremental improvement to the cost function or after a pre-set maximum number of iterations. Since the neighbouring gates can lend information to each other during spatio-temporal registration, it might be less vulnerable to local optima than spatial registration.

3 RESULTS

3.1 Data Simulation

The NCAT phantom was used to model the human anatomy during respiration [9]. A set of emission images and attenuation maps were produced throughout a normal respiratory cycle of 5 seconds. A spherical lesion of 10 mm in diameter was placed in one of six different locations, respectively the upper, middle and lower parts of the left and right lungs. A Monte-Carlo based PET simulator PET-SORTEO [10] was used to generate gated PET data from the NCAT phantom. PET-SORTEO accounts for all the major sources of noise and bias. It has been validated to be in good agreement against real acquisition [10]. The number of gate was 8 so that each gate could be regarded as static. This gate number is also being used by other researchers [11]. More gates could be used, however, it reduces the coincidence count for each gate and thus increases noise in reconstruction. Normal organ FDG activity concentration was assumed during our simulation. The PET data was output in sinogram format. Each individual gate was attenuation corrected by the corresponding attenuation map and then reconstructed by 3-D OS-EM with 4-mm Gaussian post-filtering. The reconstructed images were volumes of size $128 \times 128 \times 61$, spacing $2 \times 2 \times 2.425$ mm^3.

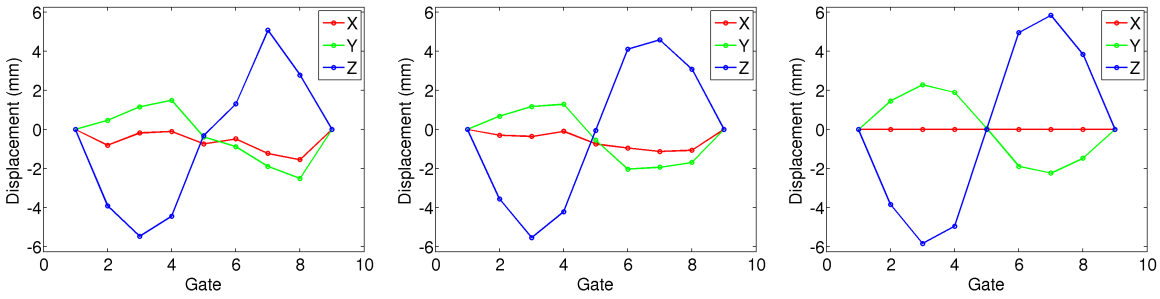

(a) Spatial registration (b) Spatio-temporal registration (c) Ground truth

Figure 2. Comparison of the displacement trajectories for spatial registration and spatio-temporal registration with ground truth. Here show the three components of the displacement along the X (left-right), Y (anterior-posterior), and Z (superior-inferior) axes respectively.

3.2 Parameter settings

We tested different spatio-temporal grid settings, including 32×32×32×8, 16×16×16×8, 8×8×8×8, and 16×16×16 ×16, where the first three numbers in the expression denote the spatial grid, and the last number denotes the temporal grid. It was found that the 16×16×16×8 grid performed best in terms of displacement trajectory estimation. Therefore, it was used for all the experiments. In addition, the grid for spatial registration was set to 16×16×16. No grid regularisation was used. The maximum iteration number was set to 50. It took approximately 20 hours to perform spatio-temporal registration on a PC with 3.20 GHz CPU and 2 GB RAM. For spatial registration, it took approximately 2 hours to register each gate, thus 14 hours for all the 7 gates.

3.3 Displacement trajectory

In this experiment, the images for all the gates were registered using both spatial registration and spatio-temporal registration. The displacements $d(i)$ at the lesion position across all the gates were computed from the resulting grid μ. The displacement trajectories were compared to the ground truth available from the NCAT phantom. Figure 2 compares the displacement trajectories for a lesion at the lower part of the left lung; as can be seen, the displacement trajectory given by spatio-temporal registration is smoother across the gates than for spatial registration. It is closer to ground truth. Table 1 lists the average errors of the estimated displacements along each axis for both registration algorithms. Spatio-temporal registration reduces the estimation errors by 0.11, 0.03, and 0.15 mm along X, Y, and Z axes respectively.

Table 1. Comparison of the average estimation errors of the displacements along the X, Y, and Z axes (unit: mm).

	Spatial			Spatio-temporal		
Lesion position	X	Y	Z	X	Y	Z
Right upper	0.35	0.39	0.66	0.20	0.28	0.54
Right middle	0.29	0.7	0.51	0.21	0.81	0.42
Right lower	0.32	0.61	0.73	0.29	0.61	0.73
Left upper	0.52	1.01	0.71	0.23	1.01	0.59
Left middle	0.33	0.51	0.69	0.31	0.54	0.41
Left lower	0.64	0.67	0.84	0.58	0.47	0.53
Mean	0.41	0.65	0.69	0.30	0.62	0.54

3.4 Motion correction

In this experiment, we registered the PET images using our spatio-temporal registration algorithm and then summed the images to give a motion corrected image. The result is compared to the uncorrected image (summation of all the images without registration) in Figure 3. It clearly shows that the corrected image displays a higher spatial resolution than the uncorrected one. The lesion in the uncorrected image is heavily blurred due to respiratory motion and hard to distinguish. In the corrected image, the lesion is clearly distinguishable. Also, we observe that in the uncorrected image, the boundary between the right lung and the liver is blurred, which may sometimes cause the problem of judging whether a lesion belongs to the lung or to the liver. However, in the corrected image, the lung and the liver are clearly separated.

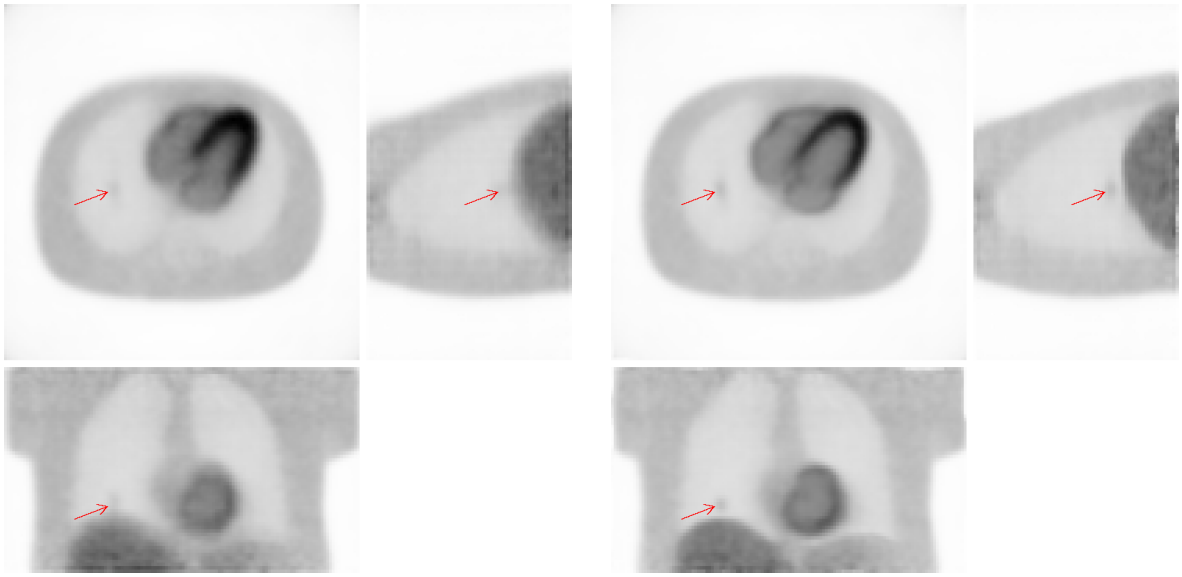

(a) Uncorrected (b) Motion corrected

Figure 3. Comparison of the uncorrected image and the motion corrected one. Here shows the axial, sagittal, and coronal views. The lesion is annotated by a red arrow.

4 CONCLUSIONS

The experimental results show that spatio-temporal registration could yield better motion estimates than spatial registration. The PET image quality is substantially improved after motion correction using our registration algorithm, compared to the uncorrected image. In the future, the performance on clinical data needs to be explored.

Acknowledgements

The authors would like to acknowledge Dr. Jérôme Declerck, Dr. Matthew Kelly, and Dr. Timor Kadir for helpful discussion. The work was supported by the DTI grant TP/16636.

References

1. E. Rohren, T. Turkington & R. Coleman. "Clinical applications of PET in oncology." *Radiology* **231(2)**, pp. 305–332, 2004.
2. J. Vansteenkiste, S. Stroobants, P. De Leyn et al. "Lymph node staging in non-small-cell lung cancer with FDG-PET scan: a prospective study on 690 lymph node stations from 68 patients." *Journal of Clinical Oncology* **16(6)**, pp. 2142–2149, 1998.
3. E. Weng, L. Tran, S. Rege et al. "Accuracy and clinical impact of mediastinal lymph node staging with FDG-PET imaging in potentially resectable lung cancer." *American Journal of Clinical Oncology* **23(1)**, pp. 47–52, 2000.
4. Y. Erdi, S. Nehmeh, T. Pan et al. "The CT motion quantitation of lung lesions and its impact on PET-measured SUVs." *Journal of Nuclear Medicine* **45(8)**, pp. 1287–92, 2004.
5. F. Lamare, M. Ledesma Carbayo, T. Cresson et al. "List-mode-based reconstruction for respiratory motion correction in PET using non-rigid body transformations." *Physics in Medicine and Biology* **52**, pp. 5187–5204, 2007.
6. M. Dawood, F. Buther, X. Jiang et al. "Respiratory motion correction in 3-D PET data with advanced optical flow algorithms." *IEEE Transactions on Medical Imaging* **27(8)**, pp. 1164–1175, 2008.
7. M. Ledesma-Carbayo, P. Mahía-Casado, A. Santos et al. "Cardiac motion analysis from ultrasound sequences using nonrigid registration: Validation against Doppler tissue velocity." *Ultrasound in Medicine & Biology* **32(4)**, pp. 483–490, 2006.
8. J. Kybic & M. Unser. "Fast parametric elastic image registration." *IEEE Transactions on Image Processing* **12(11)**, pp. 1427–1442, 2003.
9. W. Segars & B. Tsui. "Study of the efficacy of respiratory gating in myocardial SPECT using the new 4-D NCAT phantom." *IEEE Transactions on Nuclear Science* **49(3)**, pp. 675–679, 2002.
10. A. Reilhac, C. Lartizien, N. Costes et al. "PET-SORTEO: a Monte Carlo-based simulator with high count rate capabilities." *IEEE Transactions on Nuclear Science* **51(1)**, pp. 46–52, 2004.
11. F. Buther, M. Dawood, L. Stegger et al. "List mode-driven cardiac and respiratory gating in PET." *Journal of Nuclear Medicine* **50(5)**, pp. 674, 2009.